International Journal of Heat and Mass Transfer 90 (2015) 302–313

Contents lists available at ScienceDirect

International Journal of Heat and Mass Transfer

journal homepage: www.elsevier.com/locate/ijhmt

An experimental study on the effects of agitation on convective heat transfer

Smita Agrawal [a,*], Terrence Simon [a], Mark North [b], Tianhong Cui [a]

[a] Department of Mechanical Engineering, University of Minnesota, Minneapolis, MN 55455, USA
[b] Thermacore Inc., Lancaster, PA 17601, USA

ARTICLE INFO

Article history:
Received 18 November 2014
Received in revised form 26 May 2015
Accepted 27 May 2015
Available online 6 July 2015

Keywords:
Agitation
Convective heat transfer
Turbulence
Unsteady flows

ABSTRACT

In this study, agitation is produced inside a channel by a plate that is periodically oscillating normal to the channel side walls. The test channel simulates a deep-finned rectangular channel open on one end to a plenum and with a gap to allow flow over the tip of the agitator plate. The purpose of agitation is to strongly mix the near-wall flow, to thin the thermal boundary layer and to increase the convective heat transfer coefficient. Heat transfer and velocity measurements are made within different regions of the channel to study the effectiveness of such agitation. The entry region which is closest to the open end (plenum) is characterized by unsteadily driven periodic flow. The base region close to the channel base and agitator tip gap has high vortical activity and turbulent flow. The central region between the two has an unsteadily driven channel flow in one direction of oscillation and is rich in advected turbulence in the other direction. A parametric study is done to identify parameters that are critical to enhancing heat transfer. The amount of agitation produced in the channel directly scales with increasing frequency. Agitation is found to scale almost entirely with agitation velocity, the product of amplitude and frequency, with amplitude being only slightly more important than frequency in a few cases. Though this study finds application in electronics cooling where agitation can be used inside finned, air-cooled heat sinks to enhance heat transfer with walls, the results could be applied to any similar situation with such enhancement of heat or mass transfer with active surfaces. Very few experimental studies can be found in the literature on flow agitation effects on wall transport.

1. Introduction

Agitation as a mixing mechanism is used in a wide variety of applications such as in the food industry for improved heat and mass transport in stirred mixtures [1,2]. In industrial mixing, agitation is used in stirred tanks to mix fluid and solid phases. The chemical engineering industries employ numerous agitation techniques in their reactors [3–6]. Unsteadiness and turbulence generated by agitation can be used in single phase flows for improved transport from walls to fluids, e.g. in electronics cooling.

Electronics cooling technology demands rapid development to accommodate the ever-increasing heat dissipation rates of modern devices. Though phase change and liquid cooling are options, new methods of cooling with air are continually being explored. To address this, the present paper discusses a mini-channel heat sink with agitated flow for improved mixing and advanced cooling that does not resort to phase change or liquid cooling.

According to Moore, the number of transistors on a chip doubles every 1.5 or 2 years [7]. As the speed of operation and density of transistors increase, dissipation of heat from the chip rises, demanding continued attention. Without continued advancements in accommodating thermal dissipation and without a breakthrough in electronics technology, processing speed and reliability will be jeopardized. Thermal designers have traditionally used conventional fans to cool heat sink fin arrays that dissipate heat from chips in electronic devices and would like to advance air cooling technology.

The present technique employs piezoelectrically driven agitators. Many researchers have used piezoelectric actuators for cooling of electronic devices. Liu et al. [8] experimentally studied heat transfer performance of horizontal and vertical arrangements of piezoelectric fans. They concluded that heat transfer augmentation by a piezofan was due to entrained air flow during each oscillation cycle and the jet-like air stream at the fan tip. Acikalin et al. [9] characterized and optimized the performance of miniature piezoelectric fans. They evaluated changes with fan amplitude, distance to the heat source, fan length, and frequency relative to

* Corresponding author. Tel.: +1 651 280 7418.
E-mail address: agraw039@umn.edu (S. Agrawal).

http://dx.doi.org/10.1016/j.ijheatmasstransfer.2015.05.105
0017-9310/

Nomenclature

U_{peak}	agitator maximum tip speed (m/s)
A_a	amplitude of agitation, mean to peak (mm)
f	frequency of agitation (Hz)
Re	agitator tip speed Reynolds number
v	kinematic viscosity of air (m^2/s)
L	agitator to fin maximum distance when the agitator is in the mean position (mm)
H	fin length (mm)
w	agitator cavity width (mm)
π_a	agitator thickness (mm)
δ_{tip}	tip gap (mm)
h	heat transfer coefficient (W/m^2 K)
V	voltage(V)
I	current (A)
A	area of plate (m^2)
θ_s	temperature of plate (K)
P	power supplied to copper plate (W)
$Q_{net,in}$	heat flows from neighboring copper plates (W)
θ_{sink}	sink temperature (K)
U_{mean}	ensemble averaged mean velocity (m/s)
$Ui(t)$	velocity measurement at time t within the cycle number i (m/s)
U'_{RMS}	ensemble averaged RMS velocity (m/s)
t	time instant within the cycle (s)
T	oscillation cycle time (s)
a_{peak}	peak acceleration (m/s^2)

resonance. Kimber et al. [10] developed correlations that could predict thermal performance of the fan over ranges of amplitude, frequency and fan dimensions. Kimber et al. [11] studied the heat transfer performance of arrays of piezoelectric fans in their first resonant mode and noted strong dependence of heat transfer coefficient on fan pitch.

The merits of agitation as a mixing technology are known [1–6]. As a step towards improving air cooling technology, our research group employed piezoelectric technology in a different way, using piezostacks to translationally oscillate blades that agitate the flow inside heat sink channels to thoroughly mix the flow, thus improving convective heat transfer. The idea is to thin the thermal boundary layer by generating flow unsteadiness and turbulence.

Yeom et al. [12] experimentally explored agitation for an actual-scale, single channel of the heat sink. They designed an oval loop shell with a piezo actuator to drive the agitator plates for translational oscillatory motion. The channel was cooled both by agitation and throughflow. Frequencies of around 1000 Hz and 1–2 mm amplitude range were achieved. They were able to observe an improvement in heat transfer rate of around 55% due to agitation. Yu et al. [13] numerically studied factors influencing heat transfer in channels cooled by translationally oscillating agitator plates. Enhancements as high as 61% were observed. Heat transfer enhancement was found to increase with increases in amplitude and frequency. When cases of various amplitude and frequency were run, they found that agitation velocity, which is proportional to the product of amplitude and frequency, primarily effected heat transfer enhancement with amplitude being only slightly more important than frequency. Turbulence was generated in the narrow gap between the channel base and the agitator plate. This turbulence was found to play a key role in flow mixing and increasing heat transfer. Yu et al. [14] numerically studied heat transfer enhancement obtained when fan-cooled heat sinks were assisted by active devices like agitators and synthetic jets. This study was done for a single channel of the heat sink. Enhancement of around 80% was found when the performance was compared with a case of channel flow only. In another study, Yeom et al. [15] found a 91% enhancement when the throughflow-cooled channel was assisted by agitation at a frequency of 1140 Hz.

Careful agitator or heat sink design can increase the benefits that one can reap from this technology. Design studies have been done to find directions toward getting maximum heat transfer benefits with minimum agitator driving input power. Yu et al. [16] carried out a numerical study to compare the coefficient of performance when the channel is cooled by long-blade or short-blade agitators. It was found that the short blade had a better coefficient of performance compared to the long blade due to the additional vorticity generated at the edges. Significantly less power was consumed in driving a short blade. Agrawal et al. [17] numerically optimized a heat sink design. They explored the effects of the number of channels in the heat sink on heat transfer performance and agitator driving power consumption. They found that having more, narrower channels gave the best performance.

To study the agitator phenomena in detail, the effects of agitation in a single channel of a heat sink were experimentally documented by Agrawal et al. [18,19] in a Large Scale Mock Up unit that is dynamically similar to a single channel of an actual-size heat sink. They measured time-averaged heat transfer coefficients and unsteady velocities over a representative agitation cycle in various flow regions of the channel. Their study identified mechanisms of mixing within the different regions.

The aim of the present study is to explore agitation as a mixing mechanism with application to enhancing heat transfer. Aside from the study from which the present paper originates [18,19], little has been done to provide heat transfer and flow measurements with active agitation of this type. For this, experiments were done in a Large Scale Mock Up unit (described below) and parameters critical to enhanced heat transfer were identified. The results add to our understanding of the fundamentals of agitation on heat transfer.

2. Experimental setup

Fig. 1 shows the actual heat sink with agitators, an oval loop shell bow and a piezostack. As the piezostack contracts and expands, it drives the agitator assembly inside the heat sink channel via the bow motion [12,20].

A single channel of the actual heat sink might be as wide as 3–4 mm. A channel as small as this does not allow space for detailed heat transfer and velocity measurements. Since a detailed understanding of the mixing generated by agitator motion is essential for efficient design, a dynamically-similar, large-scale mock-up test facility was constructed to simulate an electronics cooling heat exchanger. The test described herein focuses on agitation, so no throughflow is present. The large scale test facility allows high resolution, both in time and space. The test channel is a rectangular channel open on one end to allow inflow and outflow of air to a plenum, as driven by agitator movement. *Thus, the facility allows the study of agitation alone, with all flow driven by the agitator itself.* Both heat transfer and velocity measurements are made in the channel cavity. Time-averaged heat transfer is measured over

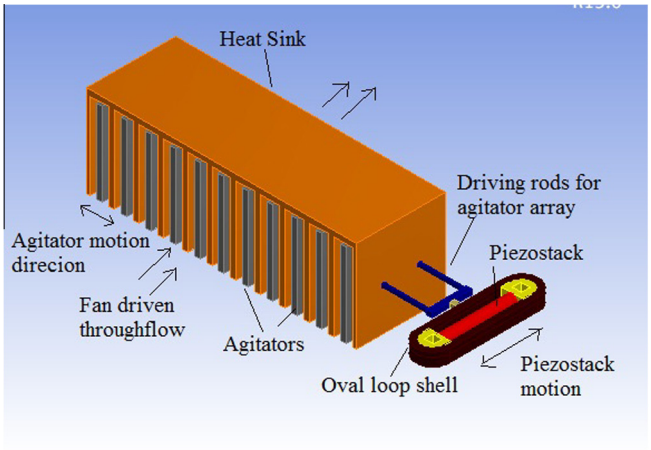

Fig. 1. Heat sink with agitator assembly of the actual heat sink.

selected regions of the channel. Velocity measurements using laser Doppler velocimetry are made within the same regions to quantify flow agitation produced by the agitator and help explain velocity field effects on heat transfer augmentation.

2.1. Apparatus

The experimental setup is shown in Fig. 2. A Scotch yoke facility is used to drive the agitator plate. A channel was simulated in the mock-up unit using polycarbonate sheets. The right wall and tip wall have copper plates embedded in them for heat transfer measurements. Plates adjacent to the test plates are for guard heating. The right wall (Fig. 4) of the channel is used for heat transfer measurements. Flow measurements are made in the channel between this wall and the agitator plate. The top wall has glass windows to allow laser beams for velocity measurements. The two edges of the agitator touching the top and bottom walls in Fig. 2, are sealed with brush seals. If we look at the channel in the direction of the arrow marked "a" in Fig. 2, we get a two-dimensional view similar to that shown in Fig. 3a. As shown in Fig. 3a, the right wall is divided into three regions: the entry, or plenum, region (nearest the open end), the central region (where an attached, unsteady boundary layer like flow is established), and the base, or gap, region (where the flow is strongly influenced by the gap flow). All the measurements are centered along these three regions. The aim is to study the performance of the agitator in generating flow

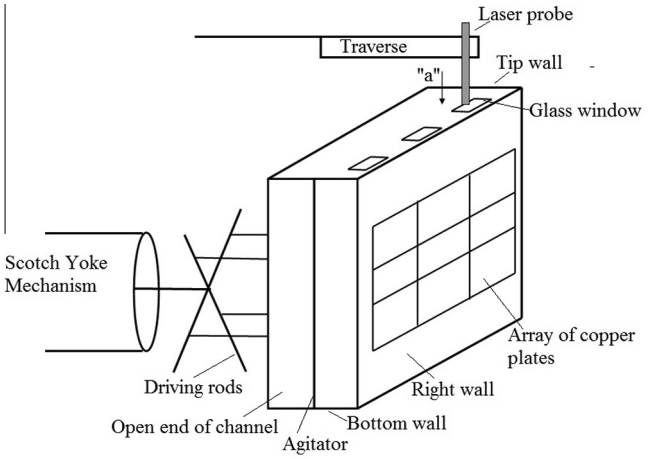

Fig. 2. Schematic view of the mock up unit with the agitator driven by a Scotch yoke mechanism ("a" shows the view of Fig. 3a).

unsteadiness and enhanced heat transfer in these three regions, which are quite different from one another. Fig. 3a shows thermocouples, $\theta 1$, $\theta 2$, and $\theta 3$ attached to the agitator plate for local air temperature measurements corresponding to sink temperatures for wall heat transfer coefficients in the three regions. Important to note in Fig. 3a is that the agitator does not extend all the way to the tip wall. There is a narrow gap between the agitator tip and the tip wall. This narrow gap, designed to simulate the gap in the actual heat sink, plays an important role in disturbing the flow by generating high-speed flows, free shear layers and vortices in the base region.

2.1.1. Scaling up

The agitator tip maximum speed Reynolds number was matched between the actual scale channel and the Large Scale

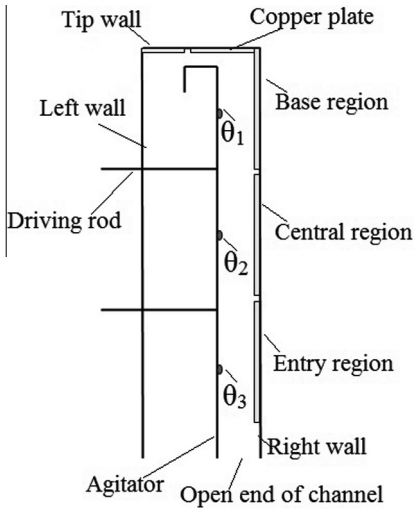

Fig. 3a. Channel in two-dimensional view (this is the view shown as "a" in Fig. 2).

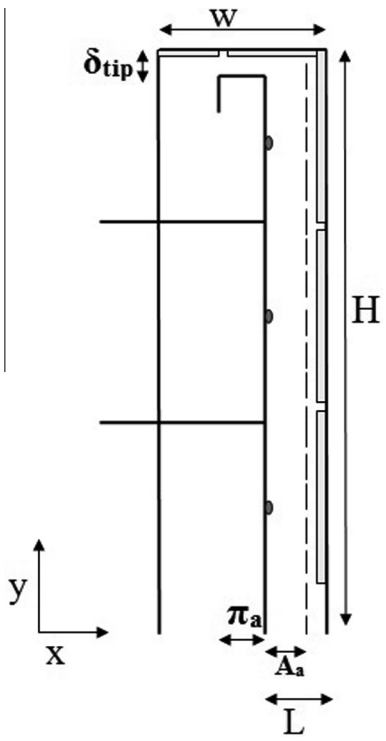

Fig. 3b. Dimensions of the channel as listed in Table 1.

Mock Up experiment. The agitator maximum tip speed is defined as:

$$U_{peak} = 2\pi A_a f \tag{1}$$

where A_a is the amplitude of the agitator and f is the frequency of agitation.

The agitator tip speed Reynolds number is defined as:

$$Re = \frac{U_{peak} L}{\nu} \tag{2}$$

where L is the agitator-to-fin maximum distance when the agitator is in the mean position. Based on this non-dimensional number, the Large Scale Mock Up experiment setup is 39 times the size of the actual heat sink channel. The parameters for the two are listed in Table 1. The locations of dimensions of the actual scale and mock up channels are shown in Fig. 3b.

2.2. Measurement method and test section details

2.2.1. Heat transfer

Fig. 4 shows details of the test plates and guard plates for the right wall. The placement of heaters and copper plates into the polycarbonate wall is shown in the edge view. The middle row of copper plates is used for heat transfer measurements. The top and bottom rows of copper plates are used for guard heating to provide appropriate boundary conditions for the middle row of test plates. Test plate 2 is used to measure the heat transfer coefficient for the entry region, plate 5 for the central region and plate 8 for the base region. The tip wall also has copper plates embedded into it to provide appropriate boundary conditions for the flow in the base region. Each of the copper plates shown in Fig. 4 has Type E thermocouples embedded into it to measure the plate temperatures. Thermocouple voltages are recorded using an Agilent 34790A data acquisition unit.

Table 1
Mockup and actual size parameter values.

Parameter	Mock up	Actual scale
Fin length (H)	640 mm	16.5 mm
Agitator cavity width (w)	132 mm	3.4 mm
Agitator thickness (π_a)	39 mm	1 mm
Amplitude (A_a)	27 mm	0.7 mm
Tip gap (δ_{tip})	19 mm	0.5 mm
Frequency (f)	0.66 Hz	1000 Hz
Agitator to fin maximum distance (L)	47 mm	1.2 mm

The plates are heated using resistance heaters glued on the backs of the plates. The voltage difference across each heater is measured. Current to the respective heater is calculated using precision resistors of nominal resistance 0.2 Ω placed in series with the power supply of each heater. The power supplied to each heater is then calculated using the measured voltage and current. Experience with these heaters indicates a unity power factor; thus $P = VI$.

At the start of the experiment, power is supplied to each copper plate through the heaters attached to it. The agitator is then allowed to oscillate inside the channel cavity to agitate the air and cool the heated plates. Meanwhile, the power supplied to each of the plates is adjusted to maintain steady state with all the plates having the same temperature, thus maintaining an isothermal wall. As shown in Fig. 3a, the local sink temperature, corresponding to each region, is measured by a thermocouple attached on the agitator in the vicinity of that region. The heat transfer coefficient is obtained as:

$$h = \frac{VI}{A(\theta_s - \theta_{sink})} \tag{3}$$

where h is the heat transfer coefficient, V is the measured voltage, I is the current, A is the area of the heated plate segment, θ_s is the surface temperature, and θ_{sink} is the local sink temperature. A small correction for power lost to neighboring plates at slightly different temperature is made based upon numerically computed plate-to-plate conductance values. Since the measurement is made far from the top and the bottom adiabatic walls, the end wall and corner effects are avoided and the flow can be said to be nominally two-dimensional. The flow domain of interest corresponds to the right side of the two-dimensional view shown in Fig. 3a.

2.2.2. Velocity measurements

Velocity measurements are made using a single-velocity-component laser Doppler probe. A TSI TR 60 series, two-component laser Doppler velocimetry system is used to make velocity measurements. The wall-parallel component of velocity is measured using the argon ion laser wavelength of 514.5 nm. The laser beam diameter is 2.65 mm.

The streamwise direction corresponds to the y axis direction shown in Fig. 3b. For this, the probe is mounted above the channel as shown in Fig. 2. Glass windows 3.2 mm (1/8 inch) thick are installed in the top polycarbonate wall to allow the laser beam to reach the measuring volume inside the channel. These windows have been installed at the three regions of interest, the entry

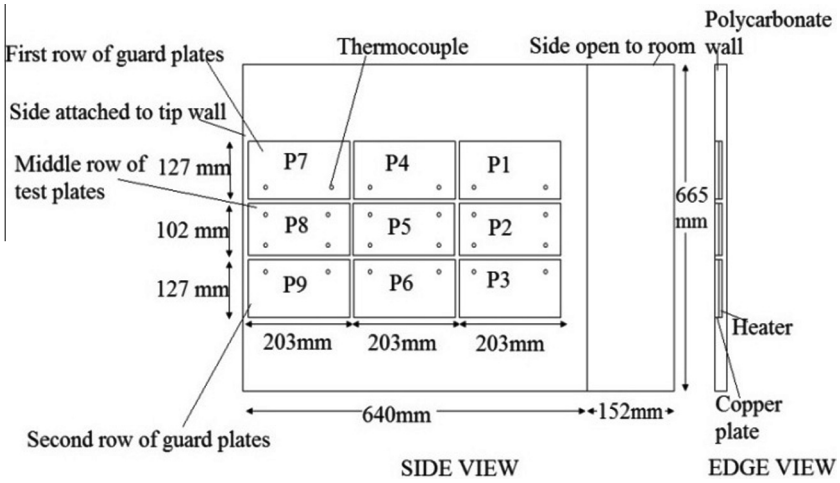

Fig. 4. Right wall of the test section.

region, the central region, and the base region. The laser probe is attached to a traverse. A water atomizer is used to seed the flow.

For any flow measurement, velocity data are collected for a number of cycles, approximately 60. An ensemble-averaged mean velocity at any instant, t, within the oscillation cycle is calculated as:

$$U_{mean}(t) = \frac{1}{n}\sum_{i=1}^{i=n} U_i(t) \tag{4}$$

where i is the cycle number and t is the particular instant within the cycle taken with reference to the start of the cycle. The quantity $U_i(t)$ is a velocity data point at that particular time for cycle number i.

The ensemble averaged RMS fluctuation of velocity is calculated as:

$$U'_{RMS}(t) = \left(\frac{1}{n}\sum_{i=1}^{n}(U_{mean}(t) - U_i(t))^2\right)^{1/2} \tag{5}$$

for time t, within the cycle.

2.3. Uncertainty and corrections

2.3.1. Uncertainty analysis

The uncertainties associated with measurements of heat transfer coefficients, h, were calculated using the equation:

$$\delta h = \left[\left(\frac{\partial h}{\partial P}\delta P\right)^2 + \left(\frac{\partial h}{\partial Q_{net,in}}\delta Q_{net,in}\right)^2 + \left(\frac{\partial h}{\partial \theta_{sink}}\delta\theta_{sink}\right)^2 + \left(\frac{\partial h}{\partial \theta_s}\delta\theta_s\right)^2 + \left(\frac{\partial h}{\partial A}\delta A\right)^2\right]^{1/2} \tag{6}$$

The uncertainties are: temperature, 0.3 K; voltage, 2% of reading, plus 2 counts; precision resistor, 1% of specified resistance of 0.2 Ω. The uncertainty associated with power is the largest term of Eq. (6). The uncertainty associated with area is small and can be neglected in comparison to the uncertainty produced by measurement of temperature and voltage. The computed uncertainty associated with each measured time-average heat transfer coefficient is in the range 6–10%.

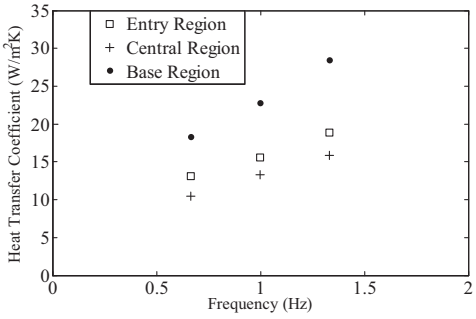

Fig. 5. Heat transfer coefficients for entry region, central region, and base region vs. frequency.

2.3.2. Natural convection correction

The aim of this study is to document the convective heat transfer performance of the agitator without contribution from other sources like natural convection. The slow speed of the mock up facility raises concern about natural convection effects that would not be in the actual heat exchanger. A test was made to assess the contribution of natural convection to the measured heat transfer coefficient. For this purpose, heat transfer coefficient measurements were made at different wall-to-sink temperature differences. The heat transfer coefficients of test plates 2, 5 and 8, used to measure heat transfer coefficients for the entry region, central region and base region, did not change with changing wall-to-sink temperature difference. Thus, it was considered that natural convection had no significant contribution to the measured heat transfer coefficient.

3. Experimental results

3.1. Heat transfer results for frequency study

Experiments were conducted at three different operating frequencies, 0.66 Hz, 1.00 Hz and 1.33 Hz in the large-scale experimental setup. The amplitude (mean-to-peak) of oscillation of the agitator for the measurements was 27 mm. The time and area averaged heat transfer coefficients are shown in Fig. 5. From Fig. 5, it can be seen that the base region shows the highest heat transfer coefficients followed by the entry region, and the central region, respectively. Also, as expected, the heat transfer coefficients increase as the frequency increases. The variation of heat transfer coefficients along the channel length can be explained by studying the variation of ensemble-averaged mean velocity and the ensemble-averaged fluctuating velocity over a cycle. The velocity results in Section 3.2 show that the ensemble-averaged mean velocity and RMS fluctuating velocities are highest in the base region, followed by the entry region and the central region. The heat transfer coefficient augmentation in each region can be attributed to two components:

(1) Flow sloshing owing to the unsteady mean velocity during a cycle.
(2) Flow turbulence characterized by the RMS fluctuating velocity at every instant within the cycle.

These results are discussed in more detail in Section 3.2.

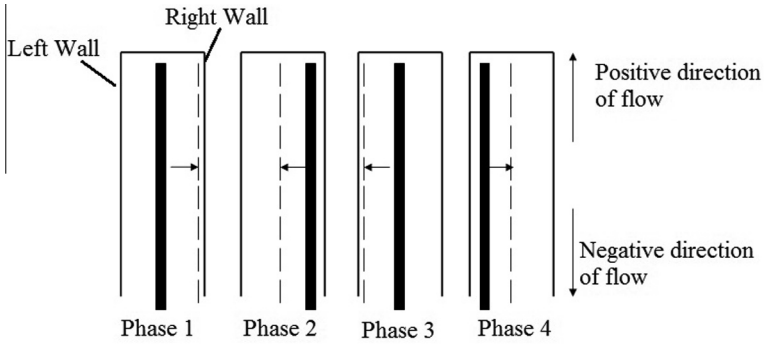

Fig. 6. Four stages in the oscillatory motion of the agitator.

3.2. Velocity characteristics along the three regions

The movement of the agitator can be divided into four different periods, as shown in Fig. 6. These are: as the agitator moves from its mean position toward the right wall (Phase 1), back from the right wall toward the mean position (Phase 2), then toward the left wall from the mean position (Phase 3) and, finally, back to the mean position (Phase 4). The figure shows the direction of the flow (negative or positive) as used in the plots in Figs. 7 and 10.

3.2.1. Entry region flow

As can be seen in Fig. 7a, during the first phase, when the agitator moves from its mean position to the right wall, the flow is driven out of the channel cavity in the negative *y* direction. As it is being pushed out during the first phase, it first accelerates and then decelerates. The flow shows some delay in response to the agitator motion just at the beginning of Phase 2; thus, it continues to be sloshed out for the initial part of Phase 2 until it achieves zero velocity and then it becomes drawn into the cavity (positive y

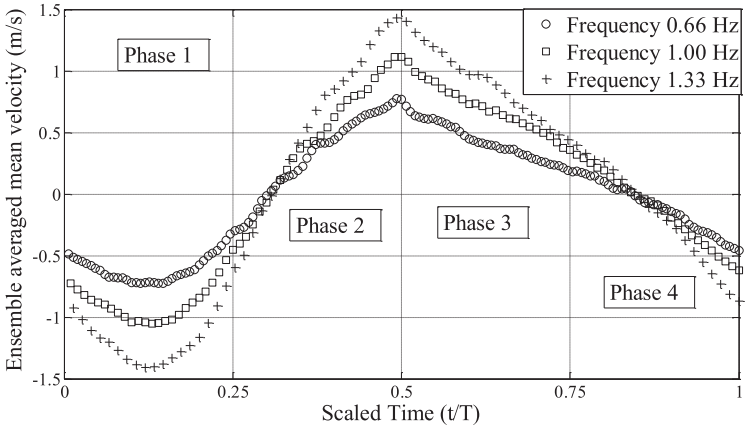

(a) Entry Region

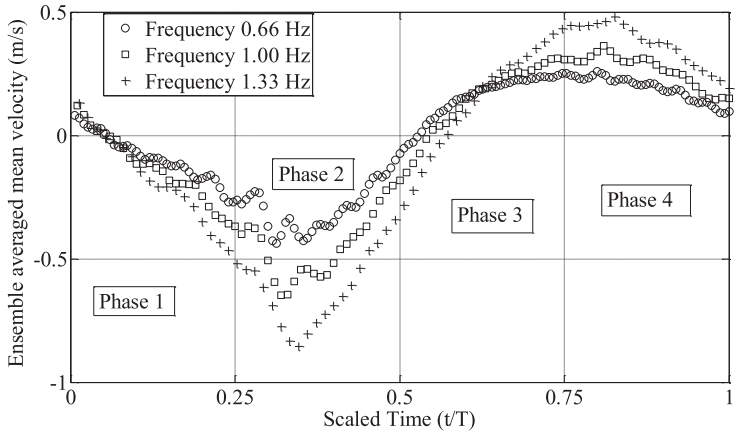

(b) Central Region

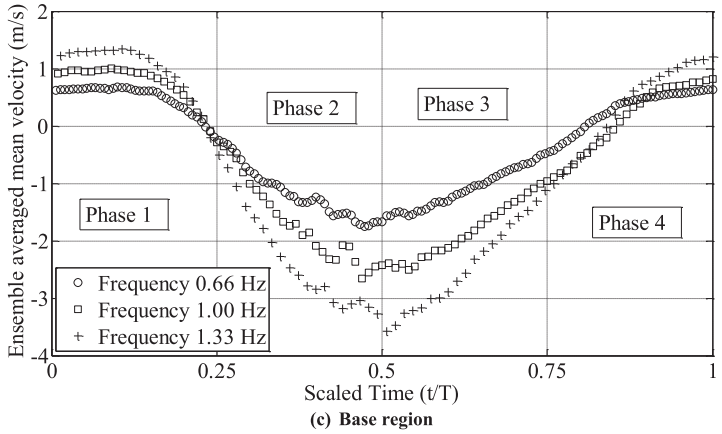

(c) Base region

Fig. 7. Ensemble-averaged mean velocity variation at three frequencies and amplitude 27 mm (mean to peak).

direction) with acceleration. The flow acceleration continues almost until the end of Phase 2. In Phase 3, as the agitator moves from its mean position to the left wall, flow continues to be drawn into the agitated channel; however, this time with deceleration. Just at the start of Phase 4, the agitator reverses direction from that of Phase 3, but the flow does not immediately respond to the change in pressure gradient set up by the agitator motion. Thus, drawing of the flow into the channel continues, with deceleration, for the initial part of Phase 4 as the agitator begins to move from the left wall to its mean position. Following the initial part of Phase 4, flow is driven out of the channel, with acceleration.

As can be seen from Fig. 8(a), velocity fluctuation increases in magnitude toward the end of the acceleration phase, in Phase 2. This increase in fluctuating velocity is carried over to the deceleration phase, as can be seen in the deceleration of Phases 3 and 4. Near the end of flow deceleration, in Phase 4, fluctuations in velocity decrease and the flow begins to stabilize as it begins accelerating in Phase 4, followed by Phase 1 of the next cycle.

3.2.2. Central region flow

The variation of velocity for the central region can be seen in Fig. 7(b). As the agitator first begins to move from its mean position to the right wall, flow direction is positive in the central region. At the start of Phase 1, when the agitator just begins to move toward the right wall, the flow becomes driven in two opposite directions. It escapes through the open (plenum) end of the channel and

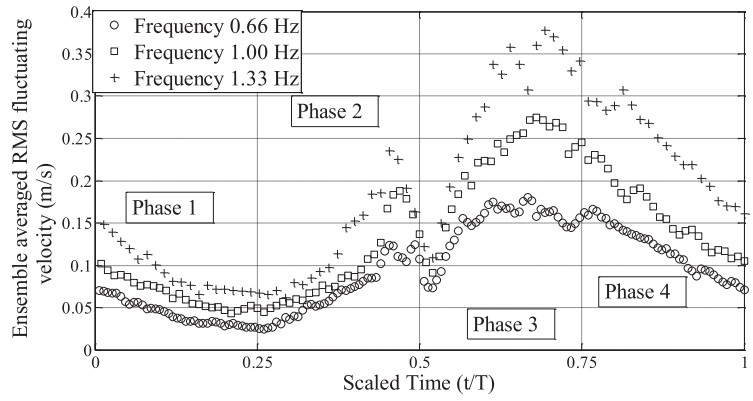

(a) Entry Region

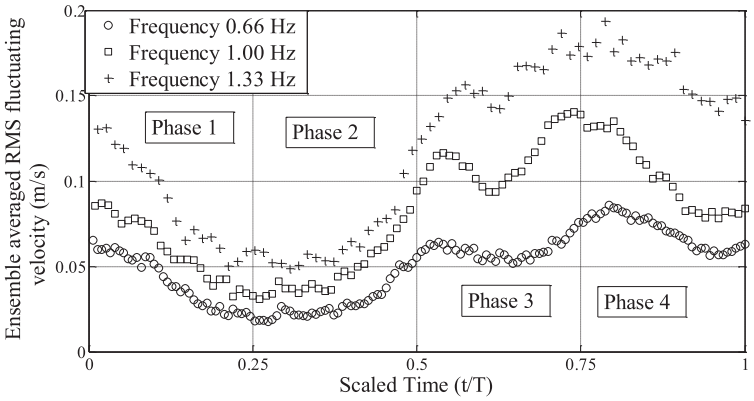

(b) Central Region

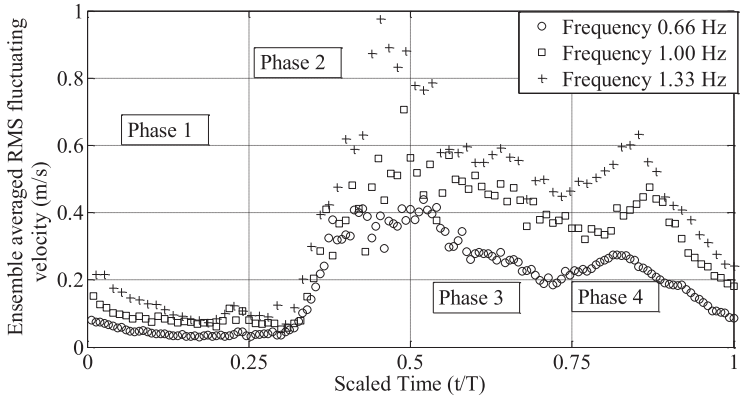

(c) Base Region

Fig. 8. Ensemble averaged RMS fluctuating velocity variation over three frequencies and amplitude 27 mm.

through the tip gap between the agitator and the tip wall. The central region, being in the center, is the region where this division takes place. As the agitator continues to move toward the right wall during the remainder of Phase 1, flow is driven out of the channel cavity (negative-*y* direction), with acceleration. The flow direction remains negative for most part of Phase 2, when the agitator starts moving back toward the mean position from nearer the right wall. As discussed in Section 3.2.1, during a major portion of Phase 2, flow is being drawn into the channel from the entry region (plenum) corresponding to the positive-*y* direction. Thus, the entry region and central region have flow moving in opposite directions in Phase 2. As the cavity is expanding due to the agitator motion, flow enters through the two extreme ends along the agitator length, the open end of the channel shown in Fig. 2 and the narrow gap between the agitator and the tip wall (base region). During Phase 3, when the agitator moves from its mean position toward the left wall, the flow direction is positive, showing that the central region is affected by the fluid drawn into the channel from the open end close to the entry region (plenum). Phase 4 also has fluid motion in the positive y-direction, though with deceleration.

The variation of fluctuating velocity (Fig. 8b) remains more or less flat for frequency 0.66 Hz. For 1.33 Hz, the variation in fluctuating velocity is more than that seen with the lower frequency. The fluctuating velocity for frequency 1.33 Hz shows an increase during the acceleration portion of Phase 3. This increase persists through most of Phase 4.

3.2.3. Base region flow

The base region variation in velocity can be seen in Fig. 7(c). The base region has the highest sloshing velocity magnitude along the channel length. This is due to the narrow gap between the agitator and the tip wall (as shown in Fig. 3a). When the agitator starts moving from its mean position to the right wall in Phase 1, flow is drawn out of the right side of the channel cavity through the narrow tip gap; therefore, the flow direction is largely positive for the first phase. During Phase 2, when the agitator starts moving away from the right wall, flow is drawn into the right side of the channel cavity over the agitator tip in the base, gap region. This drawing in of fluid (negative direction of velocity) continues throughout Phases 2 and 3 and the initial part of Phase 4, first with acceleration and then with deceleration. During the remainder of Phase 4, as the agitator continues to move from the left wall to the mean position, it pushes fluid out of the right channel cavity over the narrow tip gap corresponding to the positive y direction.

As can be seen in Fig. 8(c), the magnitudes of the fluctuating velocities change over the different phases. The magnitude of fluctuating velocity increases during the acceleration phase in Phase 2 and continues to be high for the deceleration phase of Phase 3. Toward the end of the deceleration portion of Phase 4, fluctuating velocity begins to decrease; thus, the flow begins to be stabilized as the beginning of the acceleration phase is approached.

3.2.4. A general description of the flow

In this study, we see various flow features that may be expected in an actively-agitated flow: flow separation and reattachment and flow acceleration and deceleration. It is not possible to separate the effects of these features but the measurements taken in the three regions allow discussion of effects on heat transfer of features that are stronger in their respective regions. The entry region displays separated entry flow to a channel, the central region displays unsteady boundary layer type flow and the base region displays separated flow near a bend. In general, acceleration tends to stabilize and reduce turbulence of the flow whereas deceleration tends to destabilize the flow and increase turbulence.

3.3. Velocity results-frequency study

Fig. 7(a)–(c) show the variation of ensemble averaged mean velocity with frequency for the entry region, central region and base region, respectively. The mean velocity is plotted against scaled time, since the cycle time is different for each of the three frequencies. As can be seen from the figures, the ensemble-averaged mean velocity increases with an increase in

Table 2
Agitation velocities and amplitude/frequency values for the corresponding velocities.

Agitation velocity (m/s)	Amplitude (mm) mean to peak	Frequency (Hz)
0.11	27	0.66
0.11	33	0.55
0.17	27	1.00
0.17	33	0.82
0.23	27	1.33
0.23	33	1.10

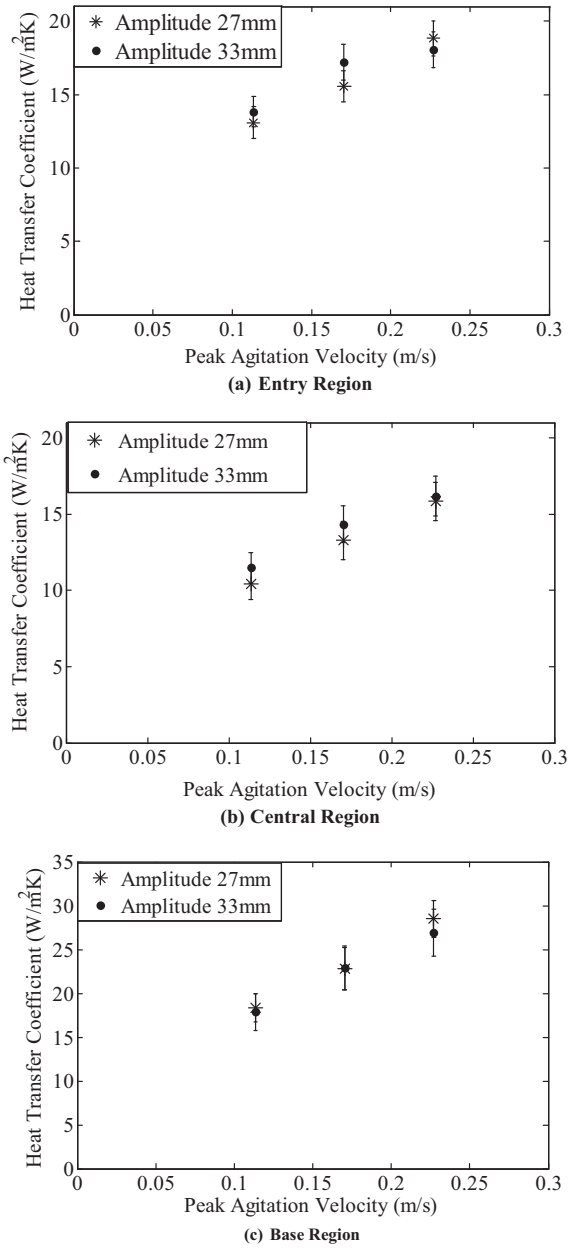

Fig. 9. Variation of heat transfer coefficient with peak agitation velocity.

frequency. There is no change in acceleration or deceleration with frequency for the entry and base regions. The mean velocity shows the same trend for each of the four phases irrespective of frequency. Thus, it can be said that the mean velocity directly scales with the frequency, for the entry and base regions. For the central region, one can see that mean velocity scales with frequency except during Phase 2, the acceleration phase, where the lower frequency curve shows some irregularities that are considered to be from an acceleration effect.

Fig. 8(a)–(c) show the variation of ensemble averaged RMS fluctuating velocity with frequency for the entry, central and base regions, respectively. As was observed for the mean velocity, the RMS fluctuating velocity more or less directly scales with frequency without showing any change in characteristics during each of the four phases. No clear acceleration effect on turbulence is visible for the central region acceleration phase (phase 2). That is, the acceleration does not visibly decrease RMS fluctuation.

3.4. Agitation velocity study

A study was done to document the effect of agitator velocity on heat transfer and velocity. The agitator peak velocity can be given as:

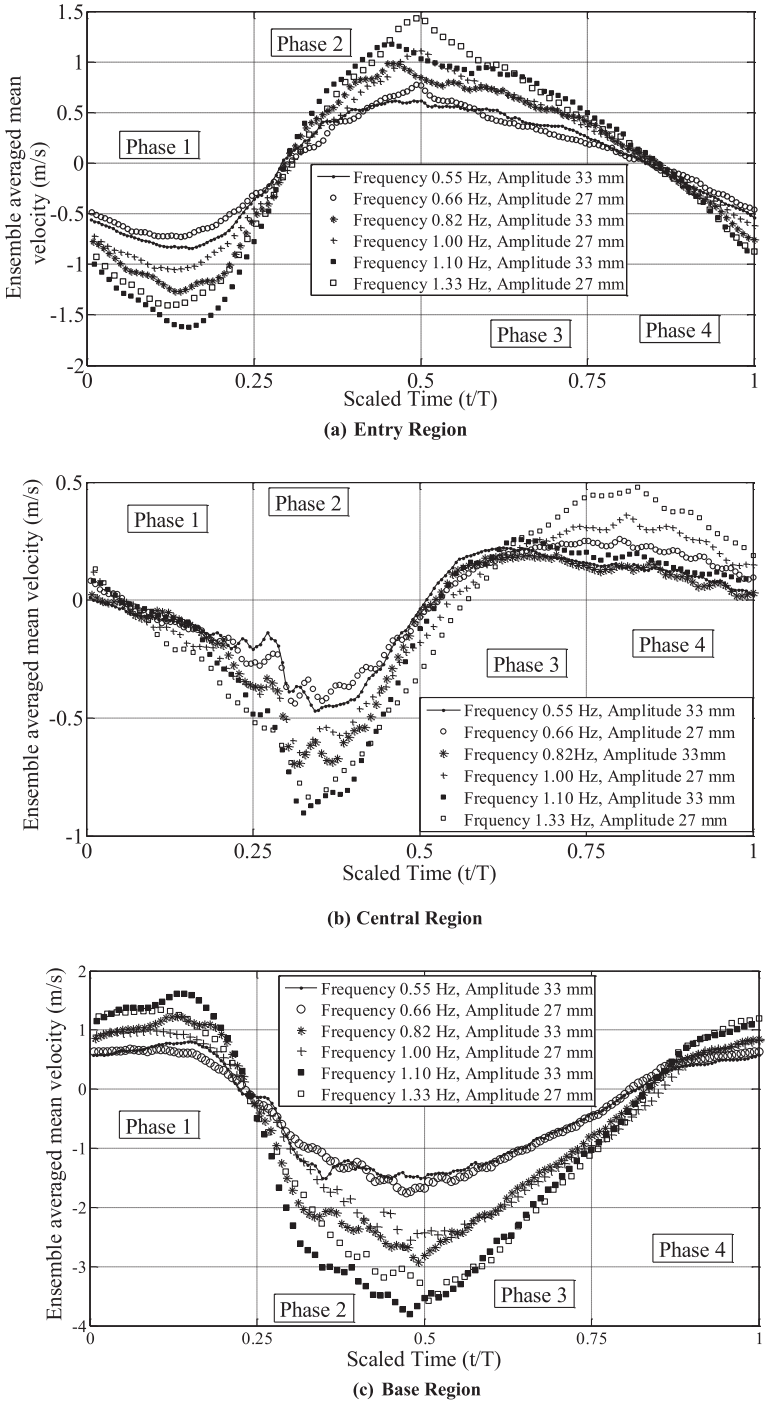

Fig. 10. Variation of ensemble averaged mean velocity with peak agitation velocity.

$$U_{peak} = 2\pi A_a f \tag{7}$$

where U_{peak} is the agitator peak velocity, A_a is the amplitude of oscillation and f is the frequency of oscillation. We are interested in discerning if the convective heat transfer is simply governed by the peak agitator velocity, irrespective of the amplitude and frequency of agitation, separately. That is, under a fixed agitator velocity, is amplitude or frequency more important than the other.

A separation of data observed for cases of the same peak agitator velocity may be attributed to acceleration effects. The peak acceleration is:

$$a_{peak} = 4\pi^2 A_a f^2 \tag{8}$$

Thus, cases with $A_a f$ matching but with higher values of f will experience larger acceleration effects.

Table 2 shows the cases studied and the corresponding agitation velocities.

From Fig. 9(a), it can be seen that, within limits of experimental uncertainty, the heat transfer coefficient for the entry region is mainly governed by agitator velocity. At a fixed agitator velocity, amplitude seems to be only slightly more effective in enhancing heat transfer, but that increase is also within limits of experimental uncertainty. From Fig. 10(a), it can be seen that the ensemble-averaged mean velocity data for the entry region show an overlap for cases with different frequency and amplitude, but

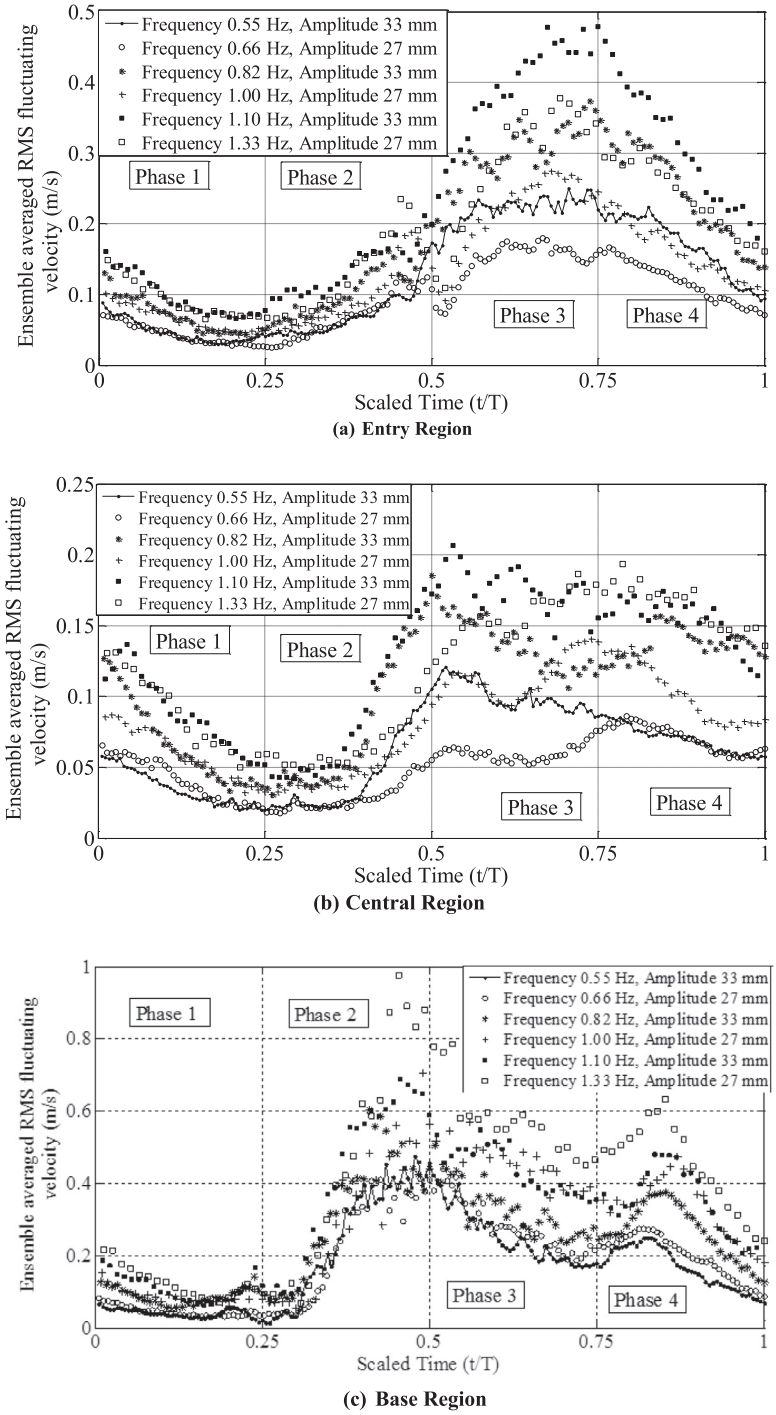

Fig. 11. Variation of ensemble averaged RMS fluctuating velocity with peak agitation velocity.

with the same agitation velocity, with slight variations during certain phases. During phase 1, the higher amplitude case has a slightly higher velocity whereas at the end of phase 2 and beginning of phase 3, the higher frequency case has a higher mean velocity. These are considered to be acceleration effects. However, these slight differences do not seem to be affecting the heat transfer coefficient strongly. From Fig. 11(a), it can be seen that during phases 3 and 4, the higher amplitude case has a higher fluctuating velocity for the entry region. During phase 3, the mean flow is decelerating, therefore turbulence production is high and the higher amplitude case is leading to the production of more turbulence. However, this slightly higher production of turbulence for one phase of the cycle does not contribute to significant enhancement in heat transfer, as seen in Fig. 9(a).

For the central region, Fig. 9(b), it can be seen that for certain agitation velocities, amplitude is slightly more effective in enhancing heat transfer, but that the increase is again within limits of experimental uncertainty. For a specific agitator velocity, the mean velocity curves (Fig. 10(b)) mostly overlap for the central region, except during phase 4, when the higher amplitude case approaches the deceleration phase faster than does the lower amplitude case. In Fig. 11(b), it can be seen that the higher amplitude case shows higher fluctuation velocities during phases 2 and 3 for the central region. Phase 2 has a decelerating mean flow for cases having the same agitation velocity but different amplitude and frequency combinations. At the same agitation velocity, phase 3 has accelerating flow for a lower amplitude and a more rapidly approaching deceleration phase for a higher amplitude. Higher amplitude favors more turbulence production during the decelerating phases. This might lead to slight increases in heat transfer as observed in Fig. 9(b), but the slight increase is within limits of experimental uncertainty.

As seen in Fig. 9(c), the base region has overlapping heat transfer coefficients at a fixed agitator velocity, except for the higher-velocity case (0.23 m/s). At the highest agitation velocity, the higher frequency case has slightly higher heat transfer coefficients, again within the limits of experimental uncertainty. Fig. 10(c) shows that the mean velocity curves generally overlap well for higher and lower amplitude cases at a fixed agitator velocity for the base region. The mean velocity is slightly higher during parts of phases 1 and 2 for the higher amplitude cases. From Fig. 11(c), for the base region, it can be seen that the fluctuating velocity curves overlap well for two cases at fixed agitation velocities, except for phases 3 and 4 when the higher frequency case shows slightly more velocity fluctuation.

In general, it can be concluded that agitator velocity is the governing factor for enhancing heat transfer, as described earlier and observed in Fig. 9(a)–(c). This is also supported by the mean and ensemble-averaged velocity plots shown in Figs. 10(a)–(c) and 11(a)–(c), with slight variations during certain phases. These slight variations are attributed to the effects of acceleration, which differ from case to case.

4. Discussion

The experimental results show that the heat transfer coefficients in the agitated flow are large and increase with increasing agitation strength. The agitator motion draws in fresh air from the surroundings and expels hot air from the channel, affecting the thermal field. But the heat transfer coefficient is established by the fluid motion, as driven by the agitator plate.

Heat transfer rates are highest in the base region, as seen in Fig. 5. This is due to the high sloshing velocity and high turbulence in the base region. Also, the strong streaking activity in the base region provides strong flow mixing via shear.

The entry region also has high sloshing velocity variations and turbulence. This leads to high heat transfer rates, although there is less streaking activity in the entry region, compared with that in the base region.

The central region has lower turbulence and sloshing velocity fluctuations than in the base region or the entry region. Also, the streaking activity in the central region is not as strong as that in the base region. This explains the lower heat transfer coefficients in the central region in Fig. 5. This region is more strongly influenced by spatial and temporal flow acceleration and deceleration.

For the entry region and the base region, high turbulence levels appear toward the end of the acceleration phase and are sustained throughout the deceleration phase. Toward the end of the deceleration phase, turbulence begins to reduce and flow becomes stabilized. Thus, the acceleration phase following the deceleration phase has a flow field with lower turbulence.

Turbulence associated with the RMS fluctuation of velocity remains uniform in the central region for the lower of the three oscillation frequencies, as can be seen in Fig. 8b. Turbulence levels increase during Phases 3 and 4 for the cases of higher oscillation frequencies, as seen in Fig. 8(b).

Fig. 5 shows that the heat transfer coefficient increases with frequency, as expected. As can be seen from Figs. 7(a)–(c) and 8(a)–(c) and mentioned in Section 3.4, the ensemble-averaged mean velocity and ensemble-averaged RMS fluctuation of velocity simply scale with frequency, without a major change in flow characteristics.

Fig. 9(a)–(c) shows that the heat transfer coefficient is governed by the product of amplitude and frequency, i.e., the agitator velocity. For all the three regions, within limits of experimental uncertainty, the heat transfer coefficient is mainly affected by the agitation velocity without amplitude or frequency being significantly more important than the other. This was also explained in Section 3.5.

5. Conclusions

A translating agitator blade can provide high heat transfer enhancement inside a channel. The agitator, with its movement back and forth, disturbs the flow sufficiently to generate mixing augmenting wall heat transfer coefficients. Test data that show the flow unsteadiness and the heat transfer enhancement due to unsteadiness are taken in a test facility that isolates, as well as one can, unsteadiness effects by having minimal steady, mean convection (minimal throughflow). This is one of very few papers that address heat transfer enhancement due to active agitation.

The test discussed in this paper creates unsteady flows having three characteristics. In the entry region, the flow is an unsteady, driven channel flow with an abrupt entry flow. In the central region, the flow is an unsteady, driven channel flow in one direction and a highly turbulent flow washed from the base region in the other direction. The central region shows the lowest heat transfer rates. The sloshing velocities are lowest in magnitude in this region. This region does experience some streaking activity; however, it is not strong enough to generate heat transfer rates as high as those in the base region. In the base region, the flow is a channel flow in one direction and a jetting and highly vortical flow (due to an upstream turning, shearing, and separating of the flow) in the other direction. The highest velocities and turbulence levels are found in the base region due to the narrow tip gap between the agitator tip and tip wall. This narrow gap leads to generation of strong vortices. The heat transfer rates are also the highest in this region, which is evident from the velocity data. The three regions have considerably different unsteadiness characteristics, each

representative of flow features one may find in an actively agitated flow.

In the entry region and the base region, increases in turbulence are found toward the end of the acceleration phase and are carried over to the deceleration phase. Decay of turbulence starts at the end of the deceleration phase when the fluid begins to accelerate. Heat transfer coefficients increase with increasing peak agitator velocity with mildly, though not significantly, higher values at higher amplitudes.

A translating blade could be oscillated in a channel through which there is a mean through-flow. The oscillation would generate unsteadiness and turbulence leading to strong mixing and augmentation of heat transfer. This is the arrangement that this research team is using in the design of a next generation heat sink for electronics cooling. The present study lends insight into the agitation effects while attempting to isolate them from the effects of mean channel through-flow.

Acknowledgment

This work was supported in part by the Defense Advanced Research Projects Agency (DARPA) MACE Program. The views expressed are those of the authors and do not reflect the official policy or position of the Department of Defense or the U.S. Government.

References

[1] E.J. Aguirre-Ezkauriatza, M.G. Galarza-Gonzalez, A.I. Uribe-Bujanda, M. Rios-Licea, F. Lopez-Pacheco, C.M. Harnandez-Brenes, M.M. Alvarez, Effect of mixing during fermentation in yogurt manufacturing, J. Dairy Sci. 91 (2008) 4454–4465.

[2] M. Dwivedi, H.S. Ramaswamy, Comparison of heat transfer rates during thermal processing under end over end and axial modes of rotation, LWT Food Sci. Technol. 43 (2010) 350–360.

[3] D. Bulnes-Abundis, M.M. Alvarez, The simplest stirring tank for laminar mixing: mixing in a vessel agitated by an off-centered angled disc, AIChE J. 59 (8) (2013) 3092–3108.

[4] Marta. Major-Godlewska, Joanna. Karcz, Agitation of a gas–solid–liquid system in a vessel with high speed impeller and vertical tubular coil, Chem. Pap. 66 (6) (2012) 566–573.

[5] J.Y. Dieulot, N. Petit, P. Rouchon, G. Delaplace, An arrangement of ideal zones with shifting boundaries as a way to model mixing processes in unsteady stirring conditions in agiatted vessels, Chem. Eng. Sci. 60 (2005) 5544–5554.

[6] L. Pakzad, F. Ein-Mozaffari, S.R. Upreti, A. Lohi, A novel and energy-efficient coaxial mixer for agitation of non-Newtonian fluids possessing yield stress, Chem. Eng. Sci. 101 (2013) 642–654.

[7] G.E. Moore, Cramming more components onto integrated circuits, Proc. IEEE 86 (1) (1998) 82–85.

[8] Sheng-Fu Liu, Ren-Tsung Huang, Wen-Jenn Sheu, Chiu.-Chuan. Wang, Heat transfer by a piezoelectric fan on a flat surface subject to the influence of horizontal/vertical arrangement, Int. J. Heat Mass Transfer 52 (2009) 2565–2570.

[9] Tolga Acikalin, Suresh V. Garimella, Raman Arvind, James Petroski, Characterization and optimization of the thermal performance of miniature piezoelectric fans, Int. J. Heat Fluid Flow 28 (2007) 806–820.

[10] Mark. Kimber, Suresh V. Garimella, Measurement and prediction of the cooling characteristics of a generalized vibrating piezoelectric fan, Int. J. Heat Mass Transfer 52 (2009) 4470–4478.

[11] Mark. Kimber, Suresh V. Garimella, Cooling performance of arrays of vibrating cantilevers, J. Heat Transfer 131 (November 2009) 1–8.

[12] T. Yeom, T.W. Simon, L. Huang, M. North, T. Cui, Piezoelectric translational agitation for enhancing forced-convection channel-flow heat transfer, Int. J. Heat Mass Transfer 55 (2012) 7398–7409.

[13] Y. Yu, T.W. Simon, S. Agrawal, M. North, T. Cui, A computational study of active heat transfer enhancement of air cooled heat sinks by actuated plates, in: Proceedings of ASME International Mechanical Engineering Congress and Exposition, IMECE 64526, Denver, USA, 2011.

[14] Y. Yu, T.W. Simon, M. Zhang, T. Yeom, M. North, T. Cui, Enhancing Heat Transfer of Air Cooled Heat Sinks using Piezoelectrically driven Agitators and Synthetic Jets, in: Proceedings of ASME International Mechanical Engineering Congress and Exposition, IMECE 64544, Denver, USA, 2011.

[15] T. Yeom, T.W. Simon, Y. Yu, M. North, T. Cui, Convective heat transfer enhancement on a channel wall with a high frequency, oscillating agitator, in: Proceedings of ASME International Mechanical Engineering Congress and Exposition, IMECE 64379, Denver, USA 2011.

[16] Y. Yu, T.W. Simon, M. North, T. Cui, Comparison of heat transfer enhancement by actuated plates in heat sink channels, in: Proceedings of the ASME 2012 Summer Heat Transfer Conference, HT 58280, Puerto Rico, USA, 2012.

[17] S. Agrawal, L. Huang, T. Simon, M. North, T. Cui, Effects of channel aspect ratio on convective heat transfer in an electronics cooling heat sink having agitation and fan induced throughflow, in: ASME 2013 Summer Heat Transfer Conference, July 2013, Minneapolis, USA.

[18] S. Agrawal, T. Simon, M. North, T. Cui, An experimental study on the effects of agitation on forced-convection heat transfer, in: ASME International Mechanical Engineering Congress and Exposition, Denver, Colorado, IMECE 2011-64558[8].

[19] S. Agrawal, T. Simon, M. North, T. Cui, An experimental study on the effects of agitation in generating flow unsteadiness and enhancing convective heat transfer, in: HT 2012-58273, ASME Summer Heat Transfer Conference, July 2012, Puerto Rico, USA.

[20] T. Yeom, T.W. Simon, M. Zhang, M.T. North, T. Cui, High frequency, large displacement, and low power consumption piezoelectric translational actuator based on an oval loop shell, Sens. Actuators A 176 (2012) 99–109.